Journal of Molecular Structure 1264 (2022) 133231

Contents lists available at ScienceDirect

Journal of Molecular Structure

journal homepage: www.elsevier.com/locate/molstr

Synthesis, characterizations of new Schiff base heterocyclic derivatives and their optoelectronic, computational studies with level II & III features of LFPs

K. Upendranath [a], Talavara Venkatesh [a,*], T.N. Lohith [b], M.A. Sridhar [b]

[a] Department of P.G. Studies and Research in Chemistry, Kuvempu University, Jnanasahyadri, Shankaraghatta, Karnataka 577451, India
[b] Department of Studies in Physics, University of Mysore, Manasagangotri, Mysuru 570006, India

ARTICLE INFO

Article history:
Received 30 November 2021
Revised 18 April 2022
Accepted 4 May 2022
Available online 5 May 2022

Keywords:
Schiff base heterocycles
Optoelectronic
Computational
LFPs

ABSTRACT

Organic Schiff base compounds with luminous characteristics are receiving attention and increasing demand for the imaging of latent fingerprints (LFPs) at crime scenes. **Sb1** and **Sb2** novel Schiff base heterocyclic compounds were synthesized and confirmed by using analytical and spectroscopic methods. The existence of both donating and accepting groups influenced the appearance of absorption bands at longer wavelength and was recorded using UV-absorption and emission spectrum in solvent media. Compounds **Sb1** and **Sb2** emit at 576 nm and 646 nm in bathochromic shift respectively. The electrochemical properties were investigated using cyclic voltammetry. Quantum chemical parameters with vibrational frequency have been estimated in density functional theory (DFT), using TD-DFT/CAM (B3LYP) approach employing 6–311++ G (d, p) basis set in the ground state. Theoretical vibrational frequency values were specifically agreed to obtained experimental values. Furthermore, FMOs, MEPs, RDG analyses and Mulliken atomic charges have been calculated. In addition, LFPs images were developed by powder dusting approach on specified materials using synthetic compounds and visualized under Visible and UV light. The level II and III properties of LFPs on the substrate were observed under light-medium with no background interference, therefore these compounds are potential materials for electroluminescent, OLEDs and forensic science applications.

1. Introduction

Latent fingerprints (LFPs) are used as physical evidence in criminal investigations because each person has different types of fingerprints. Generally, fingerprints are identified based on their level I and they are categorized into three levels. Level I deal with a whorl, arch and loop, level II consists of a core, delta and bifurcation; level III shows the sweat pores [1–3]. Commonly levels II and III occur in every human and are difficult to identify, specific powders required to develop and visualize. There are various chemical powders were carried out to visualize the LFPs such as regular, metallic and luminescent powders [4,5]. Regular powders are resinous polymers and colorant and these powders are not suitable to develop on the challenging surface and then using of metallic powders affect the human health due to the presence of metals such as lead, gold, silver etc., Both regular and metallic powders had some drawbacks like low contrast, background hindrance and low resolution [6,7]. These materials are non-luminescent properties hence low resolution occurrs and in the viewpoint of the user's health metallic powders are not suitable for development. To overcome these difficulties researchers are concentrating on organic luminescent powders to develop and visualization of LFPs and to replace regular and metallic powders [8,9].

The Schiff base is a condensation reaction between primary amine and aldehyde which leads to a formation of imines or azomethine (-HC=N-) [10]. These imines are considered as versatile organic compounds and received considerable attention in the field of pharmacological chemistry, and these are has proven their ability of pharmaceuticals as antifungal, anti-microbial, antiviral, anti-cancer and anti-TB agents [11–15]. Apart from pharmaceutical agents, the researchers have concentrated on metal-free organic Schiff base compounds to prove their ability in electroluminescent, NLO, sensor and organic photovoltaic materials [16–18]. Moreover, the π-conjugated organic compounds mainly exhibit higher luminescence properties, by having an anchoring group such as electron-accepting and electron-donating groups were acting as D-π-A moieties, this reason may help organic compounds to use in

* Corresponding author.
E-mail address: venkateshatalwar@gmail.com (T. Venkatesh).

https://doi.org/10.1016/j.molstruc.2022.133231
0022-2860/

the field of energy conversions and visualization of LFPs in the forensic science department [19–21].

Literature survey implies that quantum chemical computational studies have been carried out using density functional theory (DFT) at gaseous phase and solvent phase with different basis sets [22–24]. From theoretical studies, molecular structure and fundamental properties can be easily understands and also its helpful method to know the intrinsic and extrinsic properties compounds by the calculation of global parameters. The molecular electron transfer, vibrational frequencies, MEP and RDG, using the DFT method and gives exactness or idea to know experimental values [25–27].

Concerning the above results, we synthesized new Schiff base heterocyclic compounds using a catalytic amount of acetic acid and evaluated for optoelectronic, computational and LFPs studies.

2. Experimental

2.1. Materials and methods

Chemicals such as naphtho-[2,3-*b*] furan-2-carbohydrazide, vanillin, 2, 4 di-nitrophenol and indole-3-carboxaldehyde were purchased from Sigma Aldrich company and absolute ethanol and acetic acid brought from Hi-media. The solvents are used without further purification. FTIR spectrums are recorded on Bruker Alpha-T spectrophotometer using KBr pellets. The ^{1}H NMR (400 MHz) and ^{13}C NMR (100 MHz) were recorded Agilent NMR using DMSO–d_6 as solvent. The absorption spectrum was recorded by UV-Visible spectrophotometer (USB-4000, Ocean optics, USA) and the emission spectrum was recorded by Shimadzu RF-5301 PC spectrophotometer. The electrochemical studies were done by Cyclic Voltammograms (CHI66OD) potentiostat CH instruments using Pt wire as a counter electrode, non-aqueous Ag/AgCl as reference electrode and Glassy Carbon as a working electrode in DMSO electrolyte and PBS as supporting electrolyte. Computational studies have been carried out by DFT by using Gaussian software 09 with (DFT)/B3LYP method using 6–311++ G (d, p) basis set. In addition, LFPs images were developed on selected materials using chemical method (powder dusting) and visualized under visible and 364 nm UV-light.

2.2. General procedure

2.2.1. Synthesis of *N'-[(4*–hydroxy-*3*-methoxyphenyl*)*methylidene*]naphtho[1,2-*b*]furan-2-carbohydrazide (**Sb1**)*

An equimolar quantity of naphtho-[2,3-*b*]furan-2-carbohydrazide (1 mm) with vanillin (1 mm) using 3 drops of acetic acid in ethanol was taken in a round bottom flask and reflux with constant stirring for about 5 h. Simultaneously, the reaction was monitored by TLC (Ethyl acetate and Pet. ether). After the completion of the reaction, the reaction mixture was poured into the 100 mL flake ice with vigorous stirring for 15 min till the solid residue separated, filtered then dried and recrystallized from absolute ethanol.

Yield: 85%, mp: 320–322 °C, color: dark brown solid. FTIR (KBr, υ cm^{-1}): 3342 (OH), 3202 (NH), 2965 (OCH_3), 1663 (C=O), 1567 (C=N). ^{1}H NMR (400 MHz, DMSO–d_6, δ ppm): 11.67 (s, 1H, OH), 9.96 (s, 1H, NH), 8.88–8.09 (m, 5H, Ar-H), 8.00 (s, 1H, Ar-H), 7.90 (s, 1H, Ar-H), 7.81–7.79 (d, J = 8, 1H, Ar-H), 7.67–7.65 (d, J = 8, 1H, Ar-H), 7.50–7.48 (d, J = 8, 1H, Ar-H), 5.43 (s, 1H, CH) and 3.26 (s, 3H, OCH_3). ^{13}C NMR (100 MHz, DMSO–d_6, δ ppm): 187.91 (C = O), 148.95 (Furan C–O), 137.75, 134.34, 130.46, 129.13, 125.68, 125.21, 121.26, 110.44, 109.17, 51.01 (OCH_3). LCMS: *m/z* 360.17 [M^+]. Anal. Calcd for $C_{21}H_{16}N_2O_4$, C, 69.99; H, 4.48; N, 7.77%, found: C, 69.94; H, 4.43; N, 7.73%.

2.2.2. Synthesis of *3-{[2-(2,4*-dinitrophenyl*)*hydrazinylidene*]methyl}−1H-indole (**Sb2**)*

The compound (**Sb2**) was synthesized by the reaction of 2, 4-DNP (1 mm) and indole-3-carboxaldehyde (1 mm) and followed by synthesized compound (**Sb1**) procedure.

Yield: 86%, mp: 292–294 °C, color: red blood solid. FT-IR (KBr, υ cm^{-1}): 3280 (NH), 1587 (C = N). ^{1}H NMR (400 MHz, DMSO–d_6, δ ppm): 12.22 (s, 1H, Indole-NH), 10.04 (s, 1H, NH), 8.54–8.50 (d, J = 16, 1H, Ar-H), 8.39–8.37 (d, J = 8, 2H, Ar-H), 8.17–8.15 (d, J = 8, 2H, Ar-H), 7.98–7.97 (d, J = 4, 2H, Ar-H), 7.85 (s, 1H, Ar-H) & 7.75 (s, 1H, CH). ^{13}C NMR (100 MHz, DMSO–d_6, δ ppm): 153.70 (C=NH), 142.57, 139.09, 135.22, 133.86, 130.54, 126.07, 115.21, 113.93. LCMS: *m/z* 325.11 [M^+]. Anal. Calcd for $C_{15}H_{11}N_5O_4$, C, 55.39; H, 3.41; N, 21.53%, found: C, 55.35; H, 3.38; N, 21.49%.

2.3. Cyclic voltammetry study

Cyclic voltammetry studies were analyzed using CH Potentiostat CHI66OD electrochemical work station with help of three-electrode systems. The electrochemical cell was constructed with Glassy carbon as working electrode, Ag/AgCl (1 M KCl) as reference electrode and platinum wire as counter electrode in DMSO as electrolyte and PBS as supporting electrolyte [28]. Further, the redox onset potential was determined and using it energy molecular orbitals were calculated (E_{HOMO}-E_{LUMO}) experimentally.

2.4. Computational study

The entire quantum chemical calculations were carried out at DFT (B3LYP) method with a 6–311++ G (d, p) basis set using the Gaussian 09 software [29]. The geometry optimization and vibrational frequencies for the two heterocyclic Schiff base **Sb1** and **Sb2** compounds have been calculated. Vibrational wave number assignments and PED calculations were performed by using the results of DFT calculation and the VEDA program with symmetry considerations. Mulliken charge distribution, HOMO-LUMO energy gap and the chemical reactive descriptors were investigated and the HOMO-LUMO images were visualized using Gauss View 6.0. The MEP and RDG were calculated using the DFT results with the help of the Multiwfn 3.8 program and visualized using the Visual Molecular Dynamics (VMD) software [30–32].

2.5. LC-MS analysis

A 3 mL aliquot was injected onto a 50×4.6, 2.6 µ internal diameter DB-17 ms Accucore C18, column with a 3.0 KV capillary voltage. The column was held at 150 °C for 4.5 min, in desolation gas flow 800 L/Hr. Acetonitrile was the mobile phase A and 0.1% formic acid in water used as mobile phase B. The injector and transfer line temperature were 450 °C. The instrument used as Acquity UPLC coupled with Xevo G2-XS QT (Waters, USA.). The mass spectrometer was operated in scan mode, set to monitor ions 50–1000 m/z with a scan time of 0.9 s, following a 4.5 min solvent delay. For the fingerprint residue samples, the column temperature program was extended and held at 250 °C for 5 min and the mass spectrometer was set to monitor the scan range 50–1000 m/z with a scan time of 1 s.

2.6. Photostability of the synthesized compounds

Concentration 0.1 M of **Sb1** and **Sb2** compounds were prepared in DMSO solvent, and solution (1, 2, 3 and 4 mL) were pipetted and added to the same solution then 3 mL PBS buffer solution and made up to the mark in 10 mL volumetric flask. The maximum absorbance wavelength was determined for both compounds

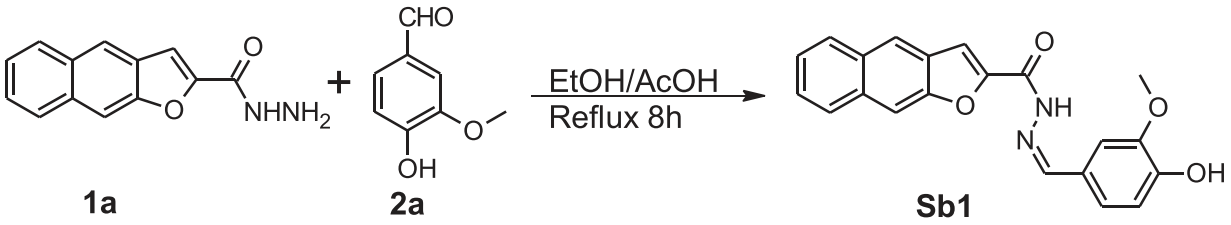

Scheme 1. Synthesis of N'-[(4–*hydroxy*-3-*methoxyphenyl*)*methylidene*]naphtho[1,2-*b*]furan-2-carbohydrazide (**Sb1**).

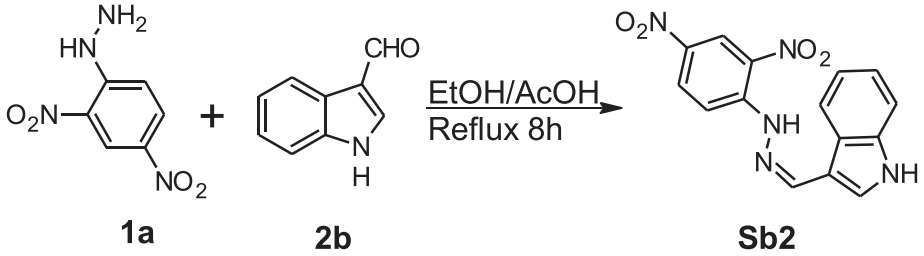

Scheme 2. Synthesis of 3-{[2-(2,4-*dinitrophenyl*)*hydrazinylidene*]methyl}−1H-indole (**Sb2**).

by changing its wavelength in colorimetric instrument. All the absorbance measurements were carried out at respective maximum absorbance wavelength at pH of 7.1 with the help of Job's method. The stability constant is

Kst $=[A_2/A_1]/1-A_1/A_2\times[C\times A_1/A_2]$where, A_1 is the absorbance at break point on extrapolation, A_2 actual absorbance of Job's plot, C is the concentration of **Sb1** and **Sb2**.

2.7. Latent fingerprints (LFPs)

A single bare hand was washed thoroughly with soapy water and cleaned them using deionized water on the first step. Different substrate such as spatula, 500 mL beaker, and aluminum foil has been collected from the laboratory, before the visualization. Synthesized Schiff base compounds **Sb1** and **Sb2** were grinded thoroughly in mortar to get a fine powder. After that, an ostrich feather fingerprint brush was used to develop the LFPs on selected non-porous materials. Developed LFPs images were captured in normal light and 365 nm UV-light using Redmi-Note 10 mobile phone and studied their level features of LFPs [33].

3. Result and discussion

3.1. Spectral characterization

In this work, we have synthesized a simple new Schiff base N'-[(4–*hydroxy*-3-*methoxyphenyl*)*methylidene*]naphtho[1,2-*b*]furan-2-carbohydrazide **Sb1** (Scheme 1), 3-{[2-(2,4-*dinitrophenyl*)*hydrazinylidene*]methyl}−1*H*-indole **Sb2** (Scheme 2) and by a conventional method using AcOH.

The structures of the desired new Schiff base heterocyclic compounds **Sb1** and **Sb2** were confirmed by recording IR, ^{1}H NMR, ^{13}C NMR and LCMS spectral data. The IR spectra of the target compound **Sb1** showed a broad stretching vibration band at 3342 cm^{-1} due to OH functionality and another stretching band at region 3202 cm^{-1} correspond to the amide (NH) group. The stretching vibration band at 1663 cm^{-1} correspond to the carbonyl group (C=O) and another band at 1567 cm^{-1} correspond to azomethine (C=N) functionality. The ^{1}H NMR spectrum of compound **Sb1** exhibited a singlet peak at δ 11.67 ppm which correspond to the OH proton of the vanillin nucleus (s, 1H, OH) and another singlet peak at δ 9.66 ppm due to amide proton (s, 1H, NH). Multiplet peaks were observed in the range of δ 8.88–7.48 ppm corresponds to aromatic protons (s, 10H, Ar-H) and a singlet peak at δ 5.43 due to CH proton (s, 1H, CH), another a singlet peak at δ 3.26 due to methoxy protons (s, 3H, OCH_3). Similarly, the carbonyl carbon (C=O) has observed in a single peak at 187.09 ppm and five-membered furan C-O carbon appeared at 148.95 ppm. Further, 137.75, 134.34, 130.46, 129.13, 125.68, 125.21, 121.26 ppm, (C=C), 110.44, 109.17 ppm corresponds to aromatic carbons. A peak obtained at 51.01 is corresponds to methoxy carbon (OCH_3). The mass spectrum showed molecular ion peak $[M]^+$ at m/z 360.0911 which correspond to the molecular weight of the compound **Sb1** in supporting information (S_1 to S_{16}) and physical parameters of **Sb1** and **Sb2** are appended in Table 1.

Table 1
Physical Properties of compounds **Sb1** and **Sb2**.

Entry	Molecular formula	Molecular weight	Yield%	Melting Point °C
Sb1	$C_{21}H_{16}N_2O_4$	360.36	85	320–322
Sb2	$C_{15}H_{11}N_5O_4$	325.27	86	292–294

3.2. UV-Visible studies

The compounds **Sb1** and **Sb2** were dissolved in three different solvents ($CHCl_3$, DMSO, and EtOH) at a concentration of 6×10^{-6} M, to study its photophysical properties. Fig. 1 shows, dual absorption peaks are appeared in the visible region with higher intensity at ~250–420 nm because of n-π^* and π-π^* transition, and aromatic conjugation. In polar solvents, due to NH functionality, the absorption bands are towards a longer wavelength which is influenced by the electron donor hydroxyl and withdrawing nitro groups as chromophores [34]. The compound **Sb1** has shown all the absorption bands at bathochromic shift by the transition between p-orbital localized on the central bond of azomethine (HC=N) and the carbonyl (C=O) group. Likewise, further, bands are located in the range of ~350–400 due to an intramolecular charge transfer (ICT) within the molecule. Similarly, compound **Sb2** has two electron-withdrawing nitro (NO_2) groups at meta and para position on the phenyl ring, which will influence their dual absorption band and increases in ICT [35]. While both the compounds have shown different absorption bands in different solvents because both compounds have different π-conjugation system and different chromophores as anchoring groups were attached. Phenomena is that the p-π conjugation effect between the lone pair electrons of O atom and π electrons of phenyl ring de-

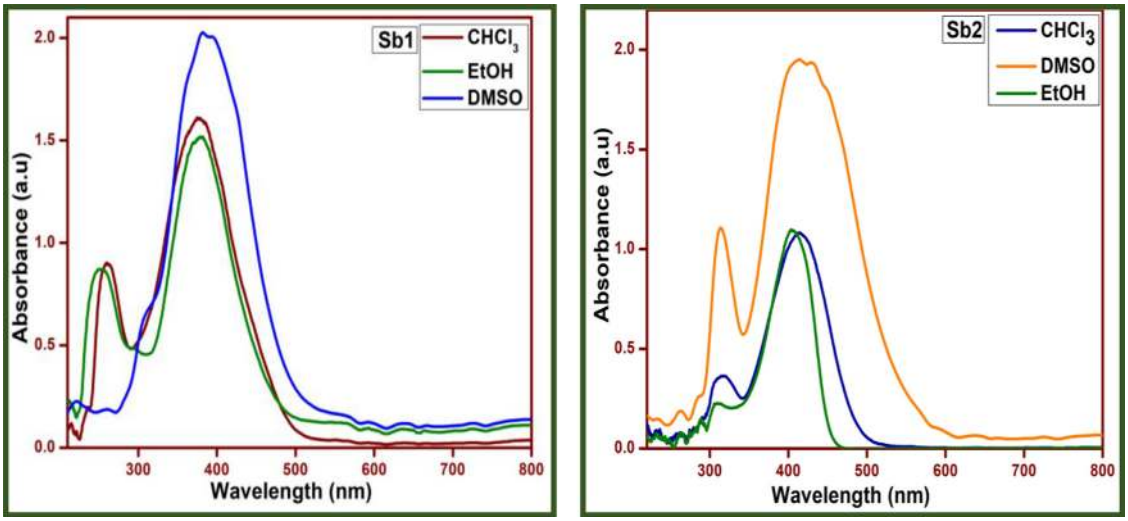

Fig 1. Electronic absorption spectra's of **Sb1** and **Sb2** in different solvents at 6 × 10^{-6} M.

Table 2
Absorption data of synthesized compounds **Sb1** and **Sb2** in different solvents.

Solvents	Entry	λ_{abs} (nm)	E_g^{OTP} (eV)*	Molar absorptivity(ε ×10^{-5} L mol^{-1} cm^{-1})
Chloroform	**Sb1**	260, 376	4.76 & 3.29	2.3
DMSO		221, 381	5.61 & 3.25	2.5
Ethanol		252, 379	4.92 & 3.27	1.6
Chloroform	**Sb2**	272, 392	4.55 & 3.16	2.6
DMSO		312, 414	3.97 & 2.99	0.3
Ethanol		257, 403	4.82 & 3.07	3.0

* $Eg = 1240/\lambda_{onset}$ eV.

crease the required energy of π-π^* transition, and it causes the π-π absorption band at redshift [36]. Compounds found better solute and solvent interaction and have good light absorption properties hence these compounds can be photonic materials and will be used in photovoltaic applications [37–40]. The further optical band gap has been calculated using Eq. (1) which are found a good energy gap between the conduction band and valance band hence these compounds easily absorb the sunlight. Absorption spectra and optical band gap values are appended in Table 2.

$$E_g = 1240/\lambda_{onset}\text{eV} \quad (1)$$

3.3. Photoluminescence studies

The Photoluminescence plays a vital role in determining the efficiency of charge carriers in semiconductors. Emission properties of **Sb1** and **Sb2** have been studied in DMSO solvent at the concentration of 6 × 10^{-6} M. Fig. 2(a) shows compounds have emitted according to the excitation wavelength. Having an electron donor and electron-withdrawing group influences a π-conjugated system to a longer wavelength and exhibits the blue emission band. Compounds **Sb1** and **Sb2** occur at the emission wavelength at 576 nm and 646 nm respectively because of NH functionality and electron density of the phenyl ring with increasing the δ-π hyperconjugation will influence to redshift. The maximum difference between absorption and emission bands is said to be stokes shifts, here the compound **Sb1** has shown larger stokes of 195 nm, while compound **Sb2** has 232 nm respectively. Both the compounds have shown higher stokes due to good solute-solvent interactions. In addition, fluorescence properties were also analyzed by the CIE systems of chromaticity coordinates. Fig. 2(b) shows that calculated CIE data with coordinates $X = 0.3093$; $Y = 0.6404$ this results in the color enhancement which is represented by the star symbol, and located at the greenish-yellow region of **Sb1** and reddish-orange at $X = 0.2996$; $Y = 0.6786$ for **Sb2**. Hence the synthesized compounds are potential materials for OLEDs applications and forensic science. Emission spectral values are summarized in Table 3.

Table 3
Emission spectral data of compounds **Sb1** and **Sb2**.

Entry	Solvent	λ_{exc} (nm)	λ_{emi} (nm)	Stoke shift
Sb1	DMSO	381	576	195
Sb2		414	646	232

3.4. CV studies

The electrochemical studies of compounds have been carried out using three-electrode cell systems in DMSO as electrolyte and PBS as supporting electrolyte with non-aqueous Ag/AgCl as reference electrode, Glassy carbon as working electrode and Platinum wire as counter electrode [41].

From the CV measurement Fig. 3) cathodic reduction peaks are observed for both the compounds **Sb1** and **Sb2** due to the presence of the carbonyl group (C=O). Moreover, nitro (NO_2) and keto group undergoes reduction. From the reduction onset potential, the lowest unoccupied molecular orbital (LUMO) was calculated using Eq. (2) and obtained −0.65 eV, −0.62 eV, −0.65 eV, and −0.68 eV respectively. Similarly, the highest occupied molecular orbital (HOMO) was calculated using Eqs. (3) and ((4). The lower the HOMO ensures the effective regeneration and recaptures the injected electron by the synthesized compounds. Hence these compounds can be used in DSSCs application [42–44]. Obtained HOMO-LUMO values are summarized in Table 4.

$$E_{(LUMO)} = -\left[E_{(redonset)} + 4.4\right]\text{eV} \quad (2)$$

$$E_{(HOMO)} = -\left[E_{(oxonset)} + 4.4\right]\text{eV} \quad (3)$$

$$E_{(HOMO)} = E_{(LUMO)} - E_g^{OPT} \quad (4)$$

3.4. Experimental quantum parameters

Experimental energy molecule (E_{HOMO}-E_{LUMO}) and calculated quantum parameters have been appended in Table 5. Ionization

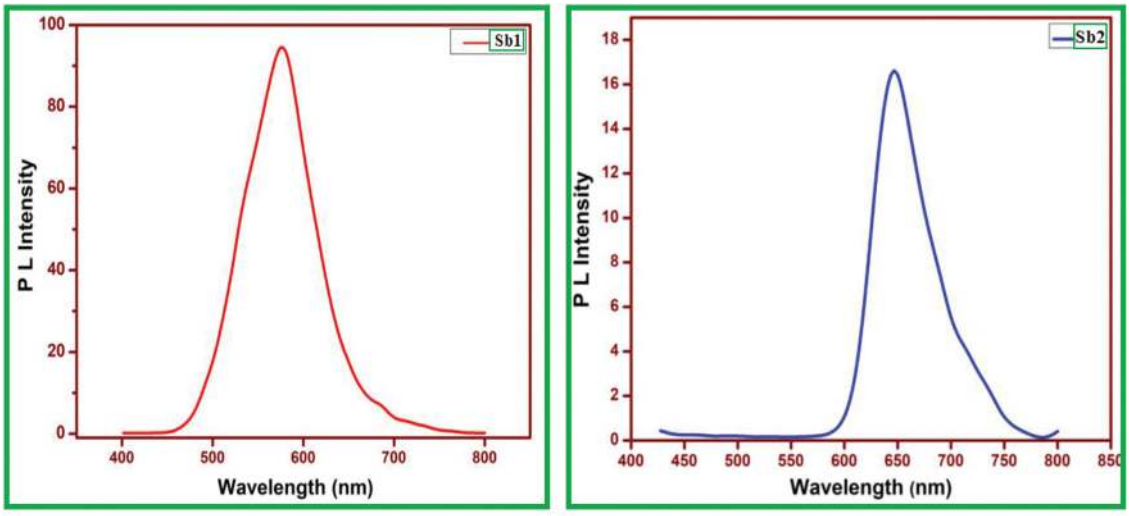

(a)

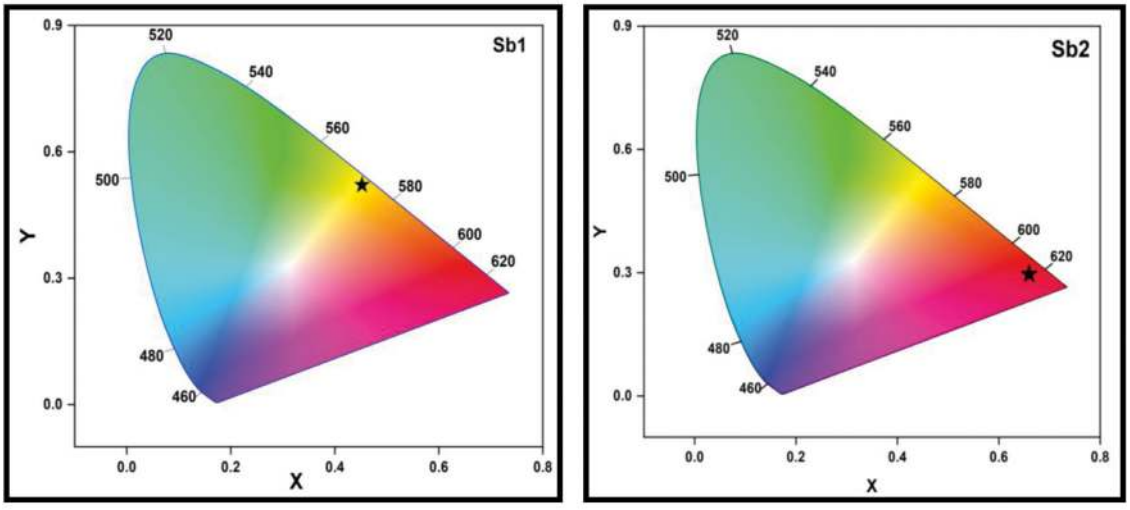

(b)

Fig 2. Photoluminescence spectra spectrum in DMSO solvent at 6×10^{-6} M of compound **Sb1** and **Sb2**
Fig. 2**(b):** CIE spectra's of compounds **Sb1 and Sb2.**

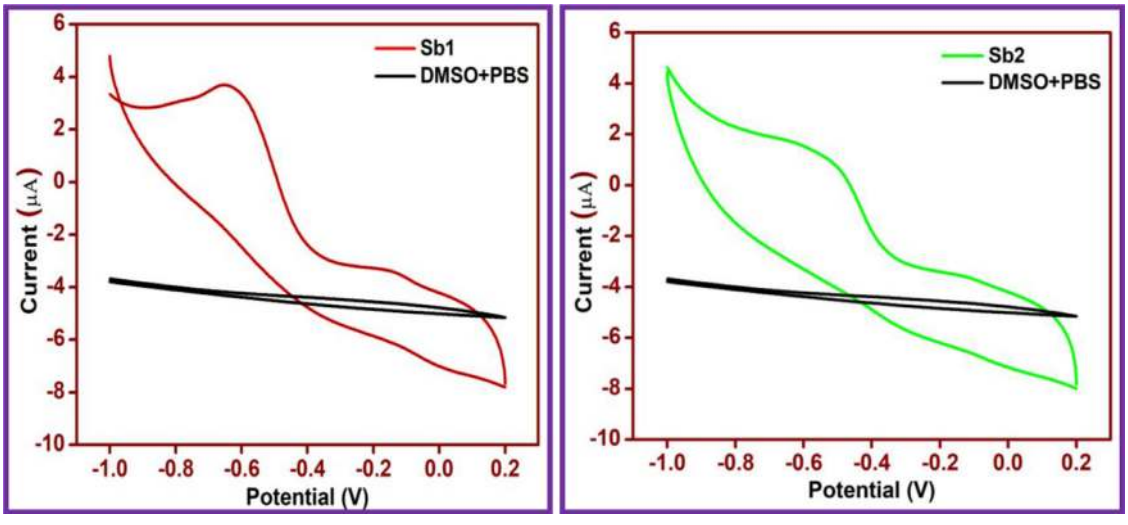

Fig. 3. A graph of cyclic voltammetry of synthesized compounds **Sb1** and **Sb2** at 6×10^{-6} M.

Table 4
Electrochemical parameters of compounds **Sb1** and **Sb2.**

Entry	Oxidation on set potential(V)	Reduction on set potential(V)	E_{HOMO} (eV)	E_{LUMO} (eV)
Sb1	–	−0.65	−7.00	−3.75
Sb2	–	−0.62	−6.77	−3.78

Table 5
Experimental quantum parameters of compounds **Sb1** and **Sb2**.

Entry	I (eV)	A (eV)	η (eV)	σ (eV)	χ (eV)	μ (eV)	ω (eV)	ΔE
Sb1	7.00	3.75	1.62	0.33	5.37	−5.37	8.90	3.25
Sb2	6.77	3.78	1.49	0.30	5.27	−5.27	9.28	2.99

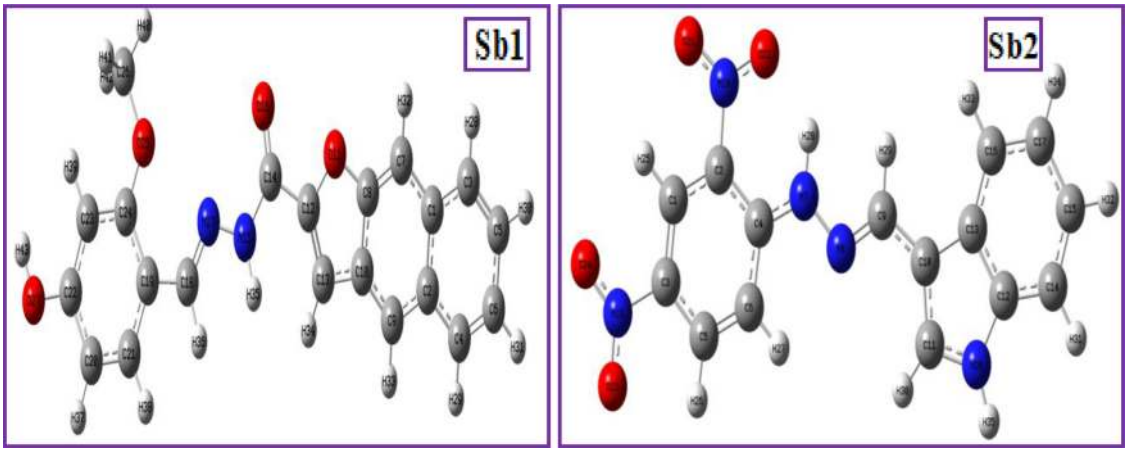

Fig. 4. Optimized structure of compounds **Sb1** and **Sb2.**

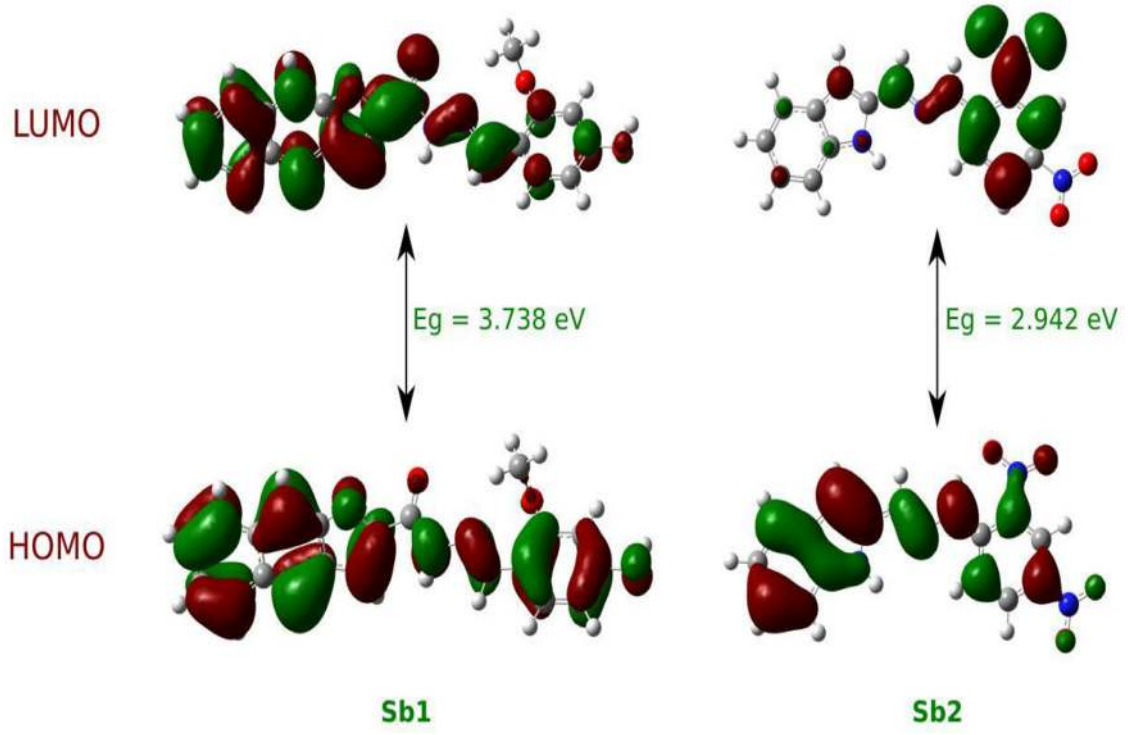

Fig. 5. Frontier molecular orbitals (EHOMO-ELUMO) synthesized compounds **Sb1** and **Sb2.**

Table 6
Frontier molecular orbitals of **Sb1** and **Sb2.**

Entry	E_{HUMO}	E_{LUMO}	ΔE
Sb1	−5.84	−2.10	3.73
Sb2	−6.04	−3.10	2.94

Table 7
Theoretical chemical parameters of compounds **Sb1** and **Sb2.**

Parameters	Values	
	Sb1	**Sb2**
Ionization energy (I) (eV)	5.8432	6.0479
Electron affinity (A) (eV)	2.1048	3.1052
Electronegativity (χ) (eV)	3.9740	4.5765
Chemical potential (μ) (eV)	−3.9740	−4.5765
Global hardness (η) (eV)	1.8692	1.4714
Global softness (σ) (eV)	0.5350	0.6796
Electrophilicity index (ω) (eV)	4.2246	7.1174

Table 8
Mullikan's atomic charges of compounds **Sb1** and **Sb2.**

Atoms		Charges	
Sb1	**Sb2**	**Sb1**	**Sb2**
C1	C1	−0.091	−0.057
C2	C2	−0.087	−0.102
C3	C3	−0.053	0.231
C4	C4	−0.071	−0.130
C5	C5	−0.061	−0.057
C6	C6	−0.061	−0.104
C7	N7	−0.007	−0.476
C8	C8	−0.114	0.122
C9	C9	0.200	−0.091
C10	C10	−0.042	0.141
C11	N11	−0.071	−0.209
C12	N12	0.081	−0.357
O13	C13	−0.279	0.305
C14	C14	0.393	−0.108
O15	C15	−0.316	−0.026
N16	C16	−0.314	0.102
N17	C17	−0.162	−0.016
C18	C18	0.151	0.103
C19	N19	−0.112	0.183
C20	O20	−0.071	−0.329
C21	O21	0.150	−0.253
C22	N22	−0.086	0.172
C23	O23	−0.106	−0.273
C24	O24	0.176	−0.270
O25		−0.370	
C26		−0.104	
O27		−0.354	

potential (E_{HOMO}) refers to the donation of electrons which gives 7.00 eV and electron affinity (E_{LUMO}) refers to acceptor electron properties which are 6.77 eV respectively. **Sb1** shows higher ionization potential due to the presence of hydroxyl group as electron donor atom conjugation, similarly, **Sb2** has shown higher ionization potential, these compounds have higher electron donor properties. Compounds also have good accepting properties which give the 3.75 eV and 3.78 eV. From the definition, the larger gap is termed as hard molecules and a smaller gap is the soft molecule, while compounds **Sb1** and **Sb2** were found in larger the energy gap hence both the compounds are said to be hard molecules. In addition, theoretical approach has been applied for compounds **Sb1** and **Sb2** to calculate the energy molecules at gaseous phase in density functional theory (DFT). The theoretical energy molecular orbital of E_{HOMO} gives the −5.80 eV and −6.04 eV, and E_{LUMO} gives −2.10 eV and −3.10 eV for both the compounds. Further, energy gap informs the compounds were soft molecule or hard molecule, here both the compounds are hard molecules due to higher in energy gap. While comparing both experimental and theoretical, experimental results are found to be higher energy values, hence synthesized compounds are having good photostability and chemical reactivity by the nature of hard molecules, therefore, synthesized compounds can be used as photosensitizer in DSSCs applications.

3.6. Computational studies

From the decades, computational studies have been attracted towards organic synthesized compounds to study of its electronic, structural properties by solving using Schrodinger equations. The geometrical optimized structure and quantum chemical parameters were examined by the DFT by using Gaussian 09 program at a gaseous phase in Gauss View 6.0.16 graphical interference with the help of (DFT)/B3LYP method using 6–311++ G (d, p) basis set [45].

3.6.1. Vibrational analysis

Theoretical vibrational analysis for synthesized compounds has been carried out at gaseous phase using (DFT)/B3LYP method using 6–311++ G (d, p) basis set and extracted from VEDA program. The FT-IR vibrational frequency values are calibrated with the default scaling factor of 0962. The targets are contained with 38 atoms with 99 to 120 fundamental (3N-6) vibrational modes which belong to C_1 point groups. The estimated FT-IR spectrum and vibrational values have been appended in the supplementary material (Fig. S_2, S_8 and Table S_1) with potential energy density.

Synthesized compounds **Sb1** and **Sb2** have different functional groups such as hydroxyl, amide, carbonyl, azomethine and aromatic groups. While compounds **Sb1** has a free hydroxyl group (O-H) stretching vibrations which are observed at 3650–3200 cm^{-1} in the IR spectrum, and hence, we observed stretching vibration at 3848 cm^{-1} theoretically in the gas phase due to intra- or inter- hydrogen molecular hydrogen bonds and hydroxyl groups were influenced by the neighboring methyl group on the phenyl ring. While in experimental we observed at 3342 cm^{-1} respectively. Similarly, both the compounds have the presence of amine (N-H) functional group which is observed at 3485 cm^{-1} and 3434 cm^{-1} in the gas phase theoretically and observed experimentally at 3202 cm^{-1} and 3280 cm^{-1} respectively.

The compound **Sb1** has the carbonyl functional group, in general, strong stretching vibration observed at 1780–1650 cm^{-1} in the aromatic ring. Here we observe strong stretching vibrations at 1779 cm^{-1} theoretical and found 1663 cm^{-1} experimentally.

The azomethine (C=N) functional group has been found 1650–1550 cm^{-1} in the IR spectrum. Both the synthesized compounds (**Sb1** and **Sb2**) have the azomethine functional group and were observed at 1679 cm^{-1} and 1617 theoretically, while we observed starching vibration at 1587 cm^{-1} and 1567 cm^{-1} respectively [46].

3.6.2. Electronic spectroscopy

For the theoretical characterization, the UV–Vis absorption spectrum was computed using the Time-Dependent Density Functional Theory (TD-DFT) at CAM-B3LYP/6–311++*G* (d, p) level of theory in the selected solvent phase. The calculated UV–Vis spectrum is shown in a supplementary file in S_3, & S_{11} and values are listed in Table S_2. The maximum absorption found at a similar position for compound **Sb1** was at 359 nm in DMSO, 358 nm in ethanol and 358 nm in chloroform, which correspondent energy of 3.45 eV, 3.46 eV and 3.46 eV, with oscillator strength of 0.40, 0.37 and 0.39. For the compound, **Sb2** has been moved further longer wavelength absorption peaks at 408 nm, 407 nm and 407 nm, correspondent energy of 3.03 eV,

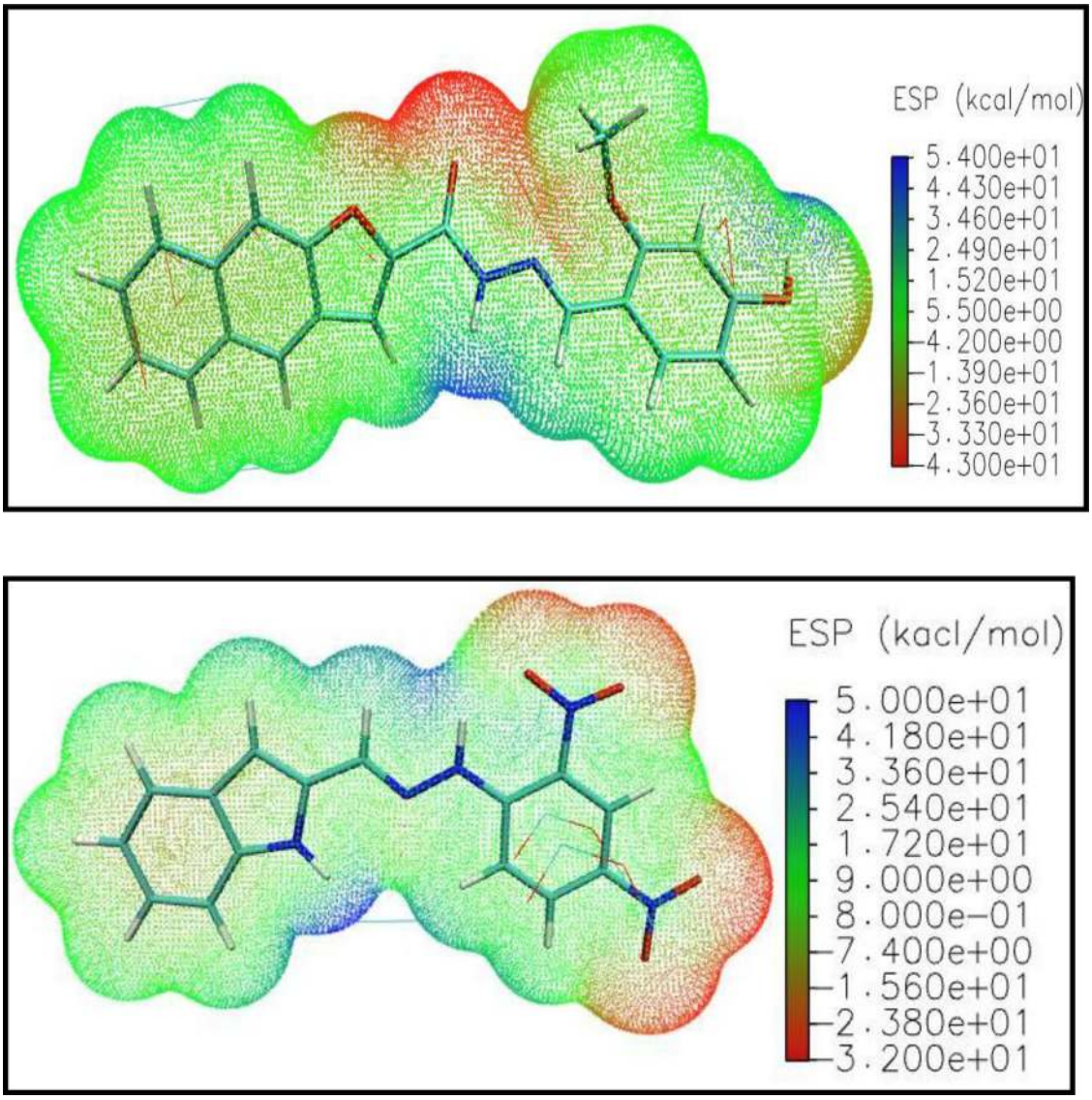

Fig. 6. Molecular electrostatic potential map of synthesized compounds **Sb1** and **Sb2.**

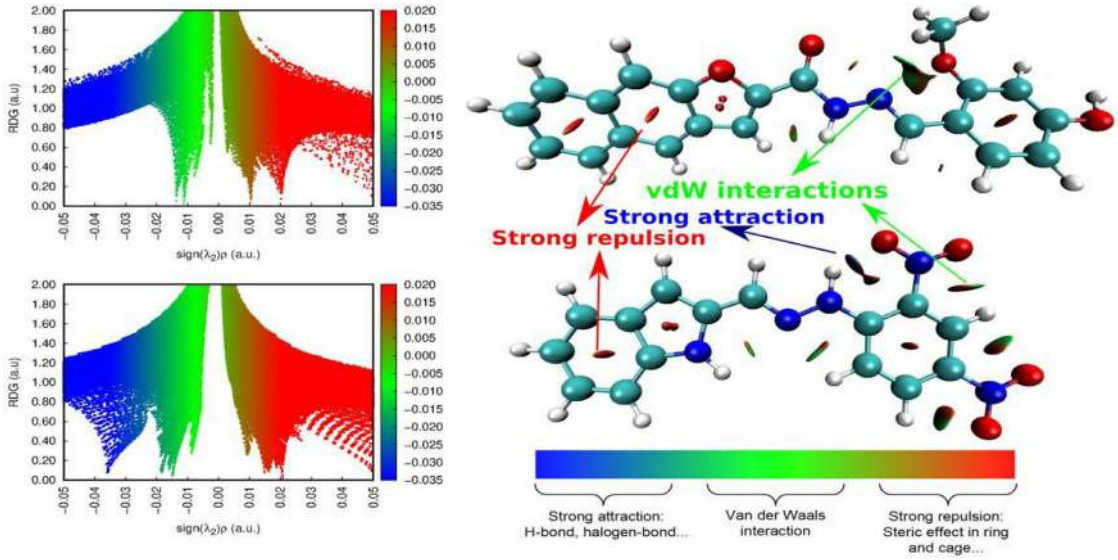

Fig. 7. RDG vs electron density scattered map and RDG isosurface map synthesized compounds **Sb1** and **Sb2**.

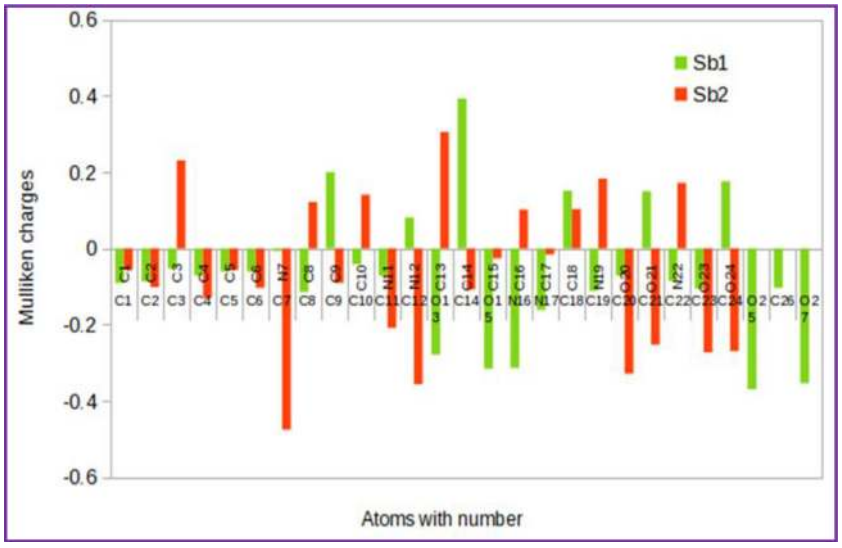

Fig. 8. Mullikan population analysis chart of synthesized compounds **Sb1** and **Sb2**.

Table 9
Theoretically computed zero-point vibrational energy, rotational constants, rotational Temperature, thermal energy, molar capacity at constant volume, entropy for **Sb1** and **Sb2.**

Parameters	Sb1	Sb2
Zero-point vibrational energy (kcal mol^{-1})	205.564	158.660
Rotational constant (GHz)	0.8368	0.540
	0.0512	0.082
	0.0490	0.071
Energy (kcal mol^{-1})		
Rotational	0.889	0.889
Translational	0.889	0.889
Vibrational	217.998	168.969
Total	219.776	170.746
Molecular capacity at constant volume (cal mol^{-1} K^{-1})		
Rotational	2.981	2.981
Translational	2.981	2.981
Vibrational	82.282	68.474
Total	88.244	74.435
Entropy (cal mol^{-1} K^{-1})		
Rotational	36.278	35.867
Translational	43.537	43.232
Vibrational	84.350	69.824
Total	164.165	148.923

Table 10
Statistical thermodynamic parameters of compounds **Sb1** and **Sb2** at various temperatures.

T (K)	S (J/mol k)		C (J/mol K)		H (J/mol K)	
	Sb1	Sb2	Sb1	Sb2	Sb1	Sb2
100	420.41	396.86	153.15	131.72	9.62	8.63
200	560.3	515.82	264.34	224.1	30.43	26.33
298.15	686.98	623.2	377.53	319.75	61.94	53.04
300	689.32	625.19	379.63	321.51	62.64	53.63
400	813.52	730.16	486.54	410.24	106.07	90.33
500	932.07	829.89	576.25	483.69	159.37	135.16
600	1043.76	923.44	648.39	542.08	220.73	186.56
700	1148.2	1010.62	706.16	588.34	288.56	243.17
800	1245.66	1091.69	752.98	625.41	361.6	303.92
900	1336.64	1167.15	791.49	655.6	438.89	368.02
1000	1421.75	1237.55	823.57	680.53	519.69	434.87

3.04 eV and 3.04 eV with oscillator strength 0.60, 0.63 and 0.59. Both the synthesized compounds found a single absorption band in the solvent system that appeared at the visible region due to π-π^* transition and aromatic conjugation. The presence of azomethine group and electron-donating and electron-withdrawing groups on phenyl rings are influenced to longer wavelength in UV-visible spectrum.

Table 11
Retention time of latent print residue (**Sb1** and **Sb2**).

Entry	Molecular weight	Abundance	Retention time
Sb1	360.17	98%	3.699
Sb2	325.11	98%	4.522

3.6.3. Geometry of the molecules

The two heterocyclic Schiff base derivatives were subjected to geometry optimization in the ground state. The optimized geometry results showed that these two molecules belong to C_1 point group symmetry. The optimized molecular structure of the two heterocyclic Schiff base compounds with an atom numbering scheme is presented in Fig. 4.

3.6.4. Frontier molecular orbitals (FMOs)

The Highest Occupied Molecular Orbital (HOMO) and Lowest Unoccupied Molecular Orbital (LUMO) are the FMOs. These orbitals are mainly involved in chemical stability. FMOs play a vital role to assign the optical and electronic properties of the materials. The ability to donate an electron is represented by HOMO, whereas LUMO, as an electron acceptor, represents the ability to obtain an electron [47,48]. The energy gaps of the two heterocyclic Schiff base compounds are found to be 3.738 eV and 2.942 eV respectively and the pictorial representation of the HOMO-LUMO of these compounds is shown in Fig. 5. The higher value of separation energy between the HOMO and LUMO explains the charge transfer interaction within the molecule. Consequently, the lower value of the bandgap is essentially a consequence of the large stabilization of the LUMO due to the strong electron acceptor ability of the electron-acceptor group. Among the two Schiff base derivatives, compound **Sb1** has a large energy gap due to less electronic conjugation compared to other molecules (**Sb2**). The other chemical reactive parameters like electrophilicity index, chemical potential, global hardness, and softness were calculated using the standard equations as given below and are listed in Tables 6 and 7.

$$\chi = -1/2(E_{LUMO}+E_{HOMO}) \quad (5)$$

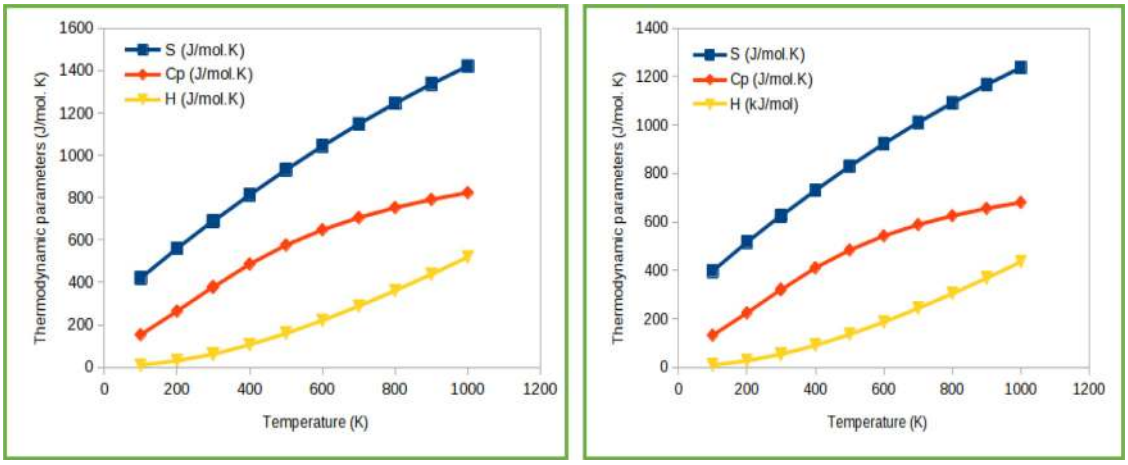

Fig 9. Correlation graph of entropy, specific heat capacity, and entropy with temperature of synthesized compounds **Sb1** and **Sb2**.

$$\mu = -\chi = 1/2(E_{LUMO}+E_{HOMO}) \quad (6)$$

$$\eta = 1/2(E_{LUMO}-E_{HOMO}) \quad (7)$$

$$\sigma = 1/2\eta \quad (8)$$

$$\omega = \mu^2/2\eta \quad (9)$$

From Table 5, one can be observed that the compound **Sb2** has a higher electrophilicity index compared to other (**Sb1**) molecules, hence the compound **Sb1** acts as a good electrophile. Also, the value of global hardness for the compound **Sb2** is lesser compared to **Sb1**. Hence the compound **Sb2** is more reactive than the **Sb1**.

3.6.5. Molecular electrostatic potential (MEP) analysis

The MEP map that is created in the space around a molecule by its nuclei and electrons is a useful tool to predict and study the reactive behavior and reactive sites present in the molecule. The MEP is related to the electronic density and is a very important descriptor for determining sites for electrophilic attack and nucleophilic reaction as well as hydrogen bonding interactions [49,50]. The MEP maps of synthesized Schiff base compounds (**Sb1** and **Sb2**) are shown in Fig. 6. With the MEP analysis, the reactive sites can be located by different color codes. The red color indicates an electron-rich site which is a negative region showing electrophilic attack while the blue color indicates an electron deficient site, which is a positive region showing nucleophilic attack. From Fig. 6, one can be observed that the negative regions in the molecules were found around the oxygen atom and the negative regions were found around the hydrogen atom attached to the nitrogen atom. The overall surface for the compound **Sb1** is 427.77 Å^3, and for **Sb2** is 359.68 Å^3 respectively. The minimum and maximum electrostatic potential for the compound **Sb2** is −43.48 kcal/mol to 54.92 kcal/mol and for **Sb2** is 32.86 kcal/mol to 50.80 kcal/mol, respectively.

3.5.6. Reduced density gradient (RDG) analysis

$RDG(r) = \frac{\Delta\rho(r)}{2(3\pi^2)^{1/3}\rho(r)^{4/3}}$ The non-covalent interactions (NCI) provide the graphical visualization of the molecular bonding and nonbonding interaction regions by the reduced density gradient and are defined by [51]

The isosurfaces exemplify the various kinds of NCI directly in real space through color codes. It enables one to distinguish the nature of the interactions attractive or repulsive and to decide their strength on a visual basis. The sign of λ_2 is used to distinguish between attractive and repulsive interactions [52]. The spike that appeared in the low density, low-density gradient region is indicative of weak interactions in the system. RDG versus (λ_2) ρ peaks provides information about the strength of interaction. From Fig. 7, one can observe the kinds of interactions present in the Schiff base compounds. The green isosurfaces are indicative of van der Waals interaction, the red colored regions show steric effect and the blue region indicates the presence of strong interaction present in the molecules **Sb1** and **Sb2**.

3.6.7. Mulliken charge analysis

The Mulliken atomic charges of synthesized compounds **Sb1** and **Sb2** were calculated by determining the electron population of each atom is defined by the basis function [53]. The Mulliken charges of the two heterocyclic Schiff base derivatives were calculated by B3LYP using a basis set 6–311G++ (d, p) and are listed in Table 8. The results can, however, be better represented in graphical form as shown in Fig. 8. From Table 8, one can observe that the charge on the C14 atom has larger than the other atoms; this is due to the attachment of a more electronegative oxygen atom. The more negative value is on O25 which is due to the attachment of the electron-donating methyl group in the **Sb1** molecule. Similarly, **Sb2** molecule, the more positive value is on the C13 atom because of the presence of neighbouring electronegative nitrogen atom and the more negative value is on N12.

3.6.8. Thermodynamic properties

Computation of thermodynamic properties and their variation with respect to temperature are important in the field of thermochemistry and chemical equilibrium. It is often employed to know these thermodynamic quantities. The total energy of a molecule is the sum of translational, vibrational, rotational and electronic energies [54]. The statistical thermochemical analyses of two Schiff base compounds (**Sb1** and **Sb2**) were carried out at room temperature of 298.15 K and one atmospheric pressure. The other thermodynamic properties viz., rotational constant, molecular capacity at constant volume and entropy are summarized in Table 9. The thermodynamic quantities such as entropy (S), enthalpy (H) and heat capacity for various temperatures (100–1000 K) were determined using the vibrational wavenumbers and these results are listed in Table 10. From Table 10, one can observe that the quantities are increasing with temperature ranging from 100 K to 1000 K as the vibrational intensities of the molecule increase with temperature. The correlation graph of thermodynamic parameters and temperature for **Sb1** and **Sb2** is shown in Fig. 9.

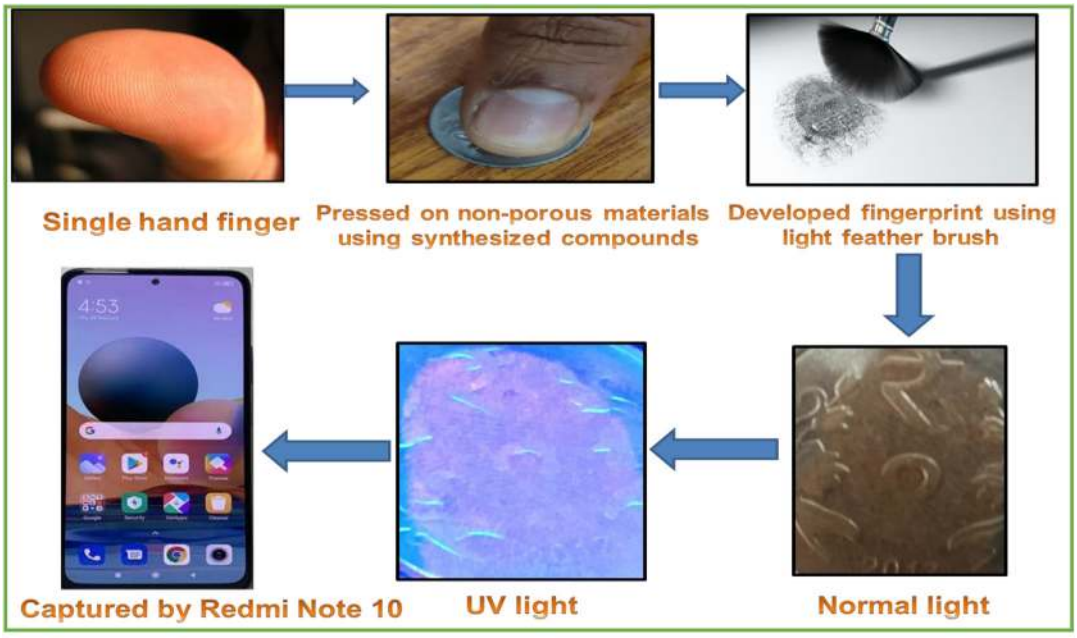

(a)

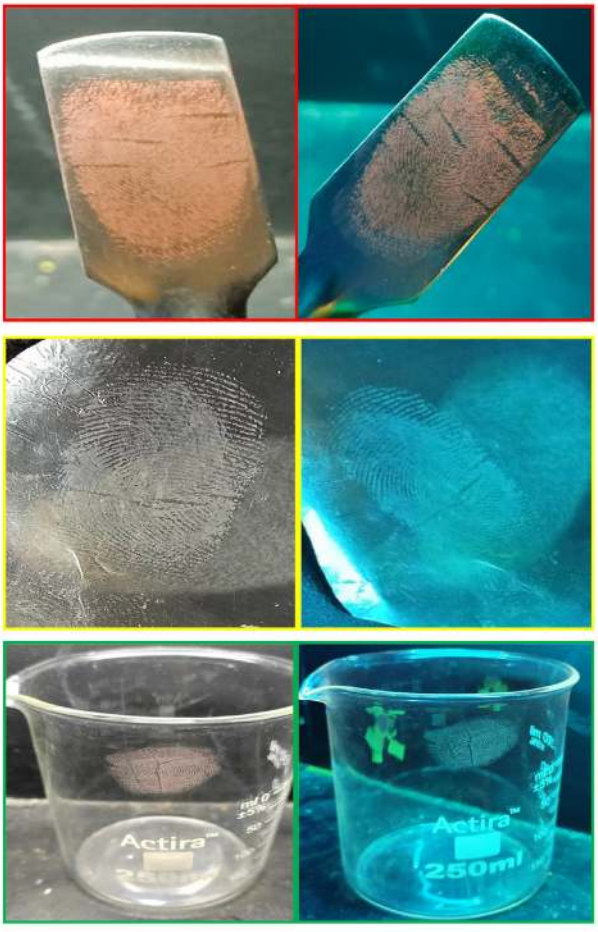

(b)

Fig. 10. (a) Schematic representation of visualizing latent fingerprints. Fig. 10 (**b**) Developed LFPs on spatula, aluminum foil and 500 mL beaker using synthesized compounds **Sb1** and **Sb2. Fig. 10(c)** Developed LFPs on spatula and ethanol bottle using synthesized compound **Sb1**
(a) bifurcation (b) short ridge (c) island.

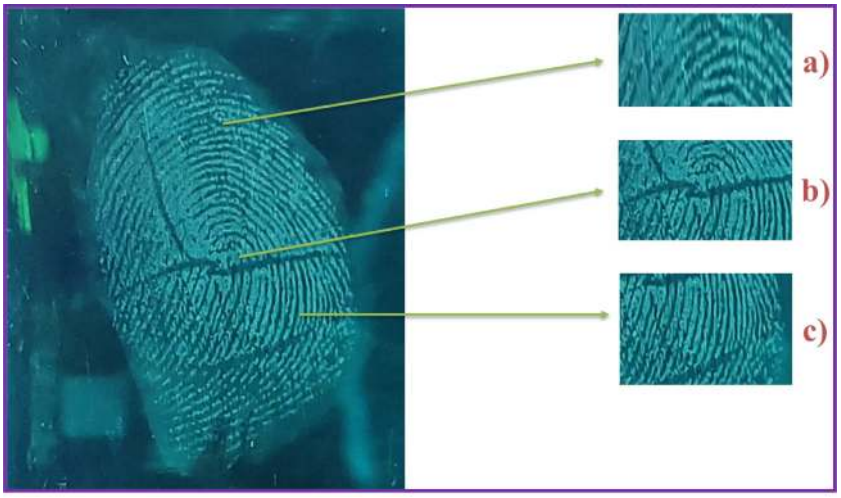

(c)

Fig. 10. Continued

3.7. Visualization of LFPs

Every human has unique fingerprints, which are helpful to use in safety lockers in banks, mobile phones, and personal identification. Other than these techniques fingerprints are used to crime spots as a preliminary method of investigation. Visualization of fingerprints at crime spots on hardcore surfaces (porous/nonporous) is the major evidence for the investigator to the identification of culprits. In general, LFPs are hard to visible to naked eyes, hence numerous methods have been followed to date for visualization such as silver nitrate spraying, powder dusting, ninhydrin fuming, iodine fuming etc., and the above methods were suffered while visualizing the LFPs such as low contrast, low sensitivity and low resolution. In these methods, for the clear visualization powder dusting method was predominantly used by every forensic analyzer due to quick and simple method was followed with fluorescence powder. When a bare finger touches the surface, some amount of sebum and sweat secreted through glands in the fingers are deposited onto the surface [55]. Three different types of natural secretion glands in the body and each gland produces a different type of sweat, namely, eccrine, sebaceous, and apocrine. Eccrine sweat glands are found all over the body at 98–99% of water, various inorganic salts (such as chloride, bromide, iodide, fluoride, and phosphate) and organic materials (such as amino acids, fatty acids and urea) surface, eccrine sweat, together with oily substances such as sebum picked up by the finger, forms an impression of the fingers ridge pattern [56] and schematic representation visualization of LFPs shown in Fig. 10(a) [57,58].

Visualization of LFPs using synthesized compounds **Sb1** and **Sb2** as organic luminescent powders and shown in Fig. 10(b) and (c). Developed LFPs are captured in normal light and UV light on different porous and nonporous surfaces such as a 500 mL beaker, spatula, aluminum foil, and white bottle, which was taken from the laboratory. Here we can observe the clear visualization of fingerprint ridges in detail in normal light and UV light, fingerprint ridges are shown in three levels, level I informs the whorls, arches, and eye, while level II informs the hooks, islands etc., and level III informs the sweat pores and scars. The compounds **Sb1** and **Sb2** exhibit the good features of level II and level III ridges without any background hindrance, the sweat pores have contained different organic and inorganic residues such as amino acids, urea, and peptides, fatty acids, and chlorides along the water. Hydrophobic amino acids contain the polar and core amino acids that play a vital role in adherence between material and synthesized compounds which shows clear and perfect images without any background hindrance. Fig. 10(c) explains clearly level II and level III ridges of latent fingerprints hence the synthesized compounds are potential materials for latent fingerprint applications and can be used in forensic science [59,60].

3.8. Latent print residue analysis

The synthesized compounds (**Sb1** and **Sb2**) were used to develop and visualization of LFPs simultaneously the compounds were analyzed from liquid chromatography-mass spectrometry (LC-MS). Latent print residues were collected from the developed surface for the analysis and compounds were determined in chromatogram based on their retention time and mass spectrum. The highest peak obtained of retention time at 3.699 which correspond to the molecular weight of **Sb1** compound 360.17 m/z and gives 98% abundance. Similarly, compound **Sb2** shows highest peak at 4.522 retention time which correspond to the molecular weight 325.11 m/z of the compound with 98% abundance. The given mass spectrum of both the compounds are listed in the supplementary file (S_8 and S_{16}) and the retention time of fingerprint residue values are listed in Table 11.

3.9. Photostability of compound

Measurement of photostability of synthesized compounds using colorimetric method at neutral pH solution and absorbance was measured. The concertation was prepared in DMSO solvent and dissolved in PBS solution at different concentrations as 1, 2, 3, and 4 mL. The stability constant was found that, 0.25 for the higher concentration of compound **Sb1** and 0.18 for compound **Sb2** at the fixed wavelength (480 nm) [61].

Therefore, **Sb1** has given higher the value as compare to **Sb2** due to higher conjugation and π-π^* interaction, from the Job's method photostability of compounds can be determined as shown in Fig. 11.

4. Conclusion

In summary, we have achieved the successfully synthesis of new Schiff base heterocyclic compounds (**Sb1** and **Sb2**). These compounds have good electron absorption properties in a highly

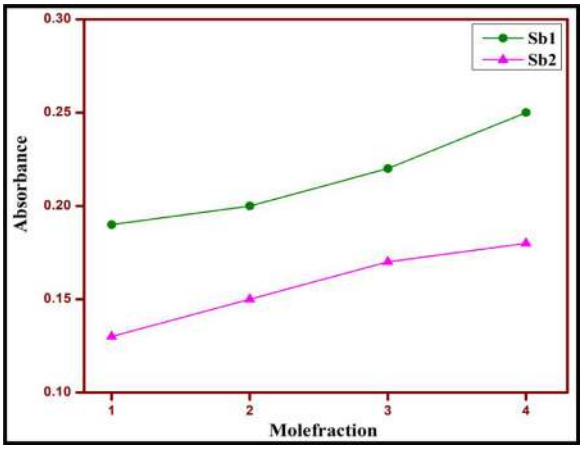

Fig. 11. Photostability of **Sb1** and **Sb2** compounds.

polar solvent by exhibiting a band at the visible region. Similarly, compounds also have better emission properties by emitting blue emissions, this emission was supported by the CIE coordinates. Redox onset potential (experimental HOMO-LUMO) reveals the electrochemical behavior and regeneration recaptures of the injected electron by the synthesized compounds. Further, computational studies such as UV-Visible and FT-IR results were in good agreement with experimental values and calculated quantum parameters reveal the higher chemical reactivity and better emission properties. Compounds showed clear observation of level II and III features of fingerprints developed on selected porous/nonporous materials. The retention time was studied from LCMS and given results are agree with obtained mass spectrum for the synthesized compounds. Hence, these can be potential materials for OLEDs, DSSCs application-oriented materials and forensic science.

CRediT authorship contribution statement

K. Upendranath: Conceptualization, Visualization, Methodology, Formal analysis, Data curation, Writing review & editing. **Talavara Venkatesh**: Conceptualization, Visualization, Methodology, Formal analysis, Data curation, Writing review & editing. **T.N. Lohith**: DFT analysis. **M.A. Sridhar**: DFT analysis.

Declaration of Competing Interest

The authors declare that they have no known competing financial interests or personal relationships that could have appeared to influence the work reported in this paper.

Acknowledgment

The authors are grateful to the Chairman, Department of PG Studies and Research in Chemistry, Kuvempu University, Shankaraghtta, Shivamogga and thankful to the University of Mysore and IISc Bangalore for providing the spectral data. The authors sincerely thank UGC, New Delhi, UGC-BSR startup Grant [F. No. F.30–486/2019 (BSR)].

Supplementary materials

Supplementary material associated with this article can be found, in the online version, at doi:10.1016/j.molstruc.2022.133231.

References

[1] R.B. Basavaraj, H. Nagabhushana, G.P. Darshan, B.D. Prasad, M. Rahul, S.C. Sharma, R. Sudaramani, K.V. Archana, Red and green emitting CTAB assisted $CdSiO_3:Tb^{3+}/Eu^{3+}$ nano powders as fluorescent labeling agents used in forensic and display applications, Dyes Pigment 147 (2017) 364–377.
[2] G.P. Darshan, H.B. Premkumar, H. Nagabhushana, S.C. Sharma, B. Daruka Prasad, S.C. Prashantha, R.B. Basavaraj, Superstructures of doped yttrium aluminates for luminescent and advanced forensic investigations, J. Alloy. Comp. 686 (2016) 577–587.
[3] C. Christophe, L. Chris, M. Pierre, S. Milutin, Fingerprints and Other Ridge Skin Impressions, CRC Press, Boca Raton, London, New York, Washington, DC, 2004 chapter 4.
[4] M. Srinivas, G.R. Vijayakumar, K.M. Mahadevan, H. Nagabhushana, H.S. Bhojya naik, Synthesis, photoluminescence and forensic applications of blue light emitting azomethine-zinc (II) complexes of bis(salicylidene)cyclohexyl-1,2-diamino based organic ligands, J. Sci. Adv. Mater. Devices 2 (2017) 156–164.
[5] R.B. Basavaraj, H. Nagabhushana, G.P. Darshan, B.D. Prasad, S.C. Sharma, K.N. Venkatachalaiah, Ultrasound assisted rare earth doped wollastonite nano powders: labeling agent for imaging eccrine latent fingerprints and cheiloscopy applications, J. Ind. Eng. Chem. 51 (2017) 90–105.
[6] M. Dhanalakshmi, H. Nagabhushana, R.B. Basavaraj, G.P. Darshan, B.D. Prasad, Surfactant-assisted $BaTiO_3:Eu^{3+}@SiO_2$ core-shell superstructures obtained by ultrasonication method:dormant fingerprint visualization and red component of white light-emitting diode applications, ACS Sustain. Chem. Eng. 6 (2018) 5214–5226.
[7] A. Sandhyarani, M.K. Kokila, G.P. Darshan, R.B. Basavaraj, B.D. Prasad, S.C. Sharma, T.K.S. Lakshmi, H. Nagabhushan, Versatile core-shell $SiO_2@SrTiO_3:Eu^{3+}$, Li^+ nano powders as fluorescent label for the visualization of latent fingerprints and anti-counterfeiting applications, J. Chem. Eng. 327 (2017) 1135–1150.
[8] M. Wang, M. Li, M. Yang, X. Zhang, A. Yu, Y. Zhu, P. Qiu, C. Mao, NIR-induced highly sensitive detection of latent fingermarks by $NaYF_4$: Yb, Er up conversion nanoparticles in a dry powder state, Nano Res. 8 (2015) 1800–1810.
[9] D. Guo, P. Wu, H. Tan, L. Xia, W. Zhou, Synthesis and luminescence properties of novel 4- (N-carbazole methyl) benzoyl hydrazone Schiff bases, J. Lumin. 131 (2011) 1272–1276.
[10] N.H. Deepthi, G.P. Darshan, R.B. Basavaraj, B.D. Prasad, H. Nagabhushana, Large-scale controlled bio-inspired fabrication of 3D $CeO_2:Eu^{3+}$ hierarchical structures for evaluation of highly sensitive visualization of latent fingerprints, Sensor. Actuator. B Chem. 255 (2018) 3127–3147.
[11] W.S. Alwan, R. Karpoormath, M.B. Palkar, H.M. Patel, R.A. Rane, M.S. Shaikh, A. Kajee, K.P. Mlisana, Novel imidazo [2,1-b]-1,3,4-thiadiazoles as promising antifungal agents against clinical isolate of cryptococcus neoformans, J. Eur. J. Med. Chem. 95 (2015) 514–525.
[12] A.T. Farghalya, G.S. Masaret, Z.A. Muhammad, M.F. Harras, Discovery of thiazole-based-chalcones and 4-hetarylthiazoles as potent anticancer agents, synthesis, docking study and anticancer activity, J. Bioorg. Chem. 98 (2020) 103761–103774.
[13] A. Kathiravan, K. Sundaravel, M. Jaccob, G. Dhinagaran, A. Rameshkumar, D.A. Ananth, T. Sivasudha, Pyrene Schiff base, photophysics, aggregation induced emission, and antimicrobial properties, J. Phys. Chem. B 118 (2014) 13573–13581.
[14] S.S. Jawoor, S.A. Patil, S.S. Toragalmath, Synthesis and characterization of heteroleptic Schiff base transition metal complexes, a study of anticancer, antimicrobial, DNA cleavage and anti-TB activity, J. Coord. Chem. 71 (2018) 271–283.
[15] V.R. Mishra, C.W. Ghanavatkar, S.N. Mali, H.K. Chaudhari, N. Sekar, Schiff base clubbed benzothiazole, synthesis, potent antimicrobial and MCF-7 anticancer activity, DNA cleavage and computational study, J. Biomol. Struct. Dyn. 38 (2019) 1772–1785.
[16] V. Nishal, D. Singh, A. Kumar, V. Tanwar, I. Singh, R. Srivastava, P.S. Kadyan, A new zinc-Schiff base complex as an electroluminescent material, J. Org. Semicond 2 (2014) 15–20.
[17] M. Kose, G. Ceyhan, M. Tumer, I. Demirtas, I. Gonul, V. McKee, Monodentate Schiff base ligands: their structural characterization, photoluminescence, anticancer, electrochemical and sensor properties, Spectrochim. Acta A Mol. Biomol. Spectrosc. 137 (2015) 477–485.
[18] K.M.P. Lokhande, K.K. Sonigara, M.M. Jadhav, D.S. Patil, S.S. Soni, N. Sekar, Multi-dentate carbazole based schiff base dyes with chlorovinylene group in spacer for dye-sensitized solar cells: a combined theoretical and experimental study, Chem. Sel. 4 (2019) 4044–4056.
[19] T. Venkatesh, K. Upendranath, Y.A. Nayaka, Development of electrochemical and optoelectronic performance of new 7-([1H-*indol*-3-*ylmethylidene*]amino)-4-methyl-2H-chromen-2-one dye, J. Solid State Electrochem. 25 (2021) 1237–1244.
[20] K.D. Seo, I.T. Choi, Y.G. Park, S. Kang, J.Y. Lee, H.K. Kim, Novel D-π-A coumarin dyes containing low band-gap chromophores for dye-sensitized solar cells, Dyes Pigment 94 (2012) 469–474.
[21] W.S. Koe, J.W. Lee, W.C. Chong, Y.L. Pang, L.C. Sim, An overview of photocatalytic degradation: photocatalysts, mechanisms, and development of photocatalytic membrane, Environ. Sci. Pollut. Res. 27 (2020) 2522–2565.
[22] C. Hachem, F. Bocquillon, O. Zahraa, M. Bouchy, Decolourization of textile industry wastewater by the photocatalytic degradation process, Dyes Pigment 49 (2001) 117–125.
[23] A. Badshah, M.F. Nazar, A. Mahmood, W. Ahmed, M. Imran Abdullahe, M.N. Zafar, U.A. Rana, Synthesis, characterization of novel cyclohexenone derivatives and computation of their optical response, J. Mol. Struct. 5 (2014) 103–110.
[24] H.S. Sumrra, F. Mushtaq, M. Khalid, MAs Raza, M.F. Nazar, B. Ali, A.A.C. Braga, Synthesis, spectral characterization and computed optical analysis of potent

triazole based compounds, Spectrochim. Acta A Mol. Biomol. Spectrosc. 5 (2017) 197–207.
[25] S.H. Sumrra, W. Zafar, M.L. Asghar, F. Mushtaq, M.A. Raza, M.F. Nazar, M.A. Nadeem, M. Imran, S. Mumtaz, Computational investigation of molecular structures, spectroscopic properties, cholinesterase inhibition and antibacterial activities of triazole Schiff bases endowed metal chelates, J. Mol. Struct. 1238 (2021) 12382–12394.
[26] A. Mahmood, M.I. Abdullah, M.F. Nazar, Quantum chemical designing of novel organic non-linear optical compounds, Bull. Korean Chem. Soc. 35 (2014) 1391–1397.
[27] J. Ashraf, E.U. Mughal, A. Sadiq, M. Bibi, N. Naeem, A. Ali, A. Massadaq, N. Fatima, A. Javid, M.N. Zafar, B.A. Khan, M.F. Nazar, A. Mumtaz, M.N. Tahir, M. Mirzaei, Exploring 3-hydroxyflavone scaffolds as mushroom tyrosinase inhibitors: synthesis, X-ray crystallography, antimicrobial, fluorescence behaviour, structure-activity relationship and molecular modelling studies, J. Biomol. Struct.Dyn. 39 (2021) 7107–7122.
[28] N.A. El-Ghamaz, M.A. Diab, A.A. El-Bindary, A.Z. El-Sonbati, H.A. Seyam, Geometrical structure and optical properties of antipyrine Schiff base derivatives, Mater. Sci. Semicond. 27 (2014) 521–531.
[29] D.V. Geetha, F.H. Al-Ostoot, Y.H.E. Mohammed, M.A. Sridhar, S.A. Khanum, N.K. Lokanath, Synthesis, elucidation, Hirshfeld surface analysis, and DFT calculations of 4-chloro-N-[2-(2-1H-*indol*-3-*yl*-*acetylamino*)-*phenyl*]-benzamide, J. Mol. Struct. 1178 (2019) 384–393.
[30] K. Singh, R. Kataria, Crystal structure, Hirshfeld surface and DFT based NBO, NLO, ECT and MEP of benzothiazole based hydrazone, Chem. Phys. 538 (2020) 110873–110884.
[31] M. Prabhaharan, A.R. Prabakaran, S. Gunasekaran, S. Srinivasan, DFT studies on vibrational spectra, HOMO–LUMO, NBO and thermodynamic function analysis of cyanuric fluoride, Spectrochim. Acta A Mol. Biomol. Spectrosc. 136 (2015) 494–503.
[32] S.M. Hiremath, A. Suvitha, N.R. Patil, C.S. Hiremath, S.S. Khemalapure, S.K. Pattanayak, K. Obelannavar, Molecular structure, vibrational spectra, NMR, UV, NBO, NLO, HOMO-LUMO and molecular docking of 2-(4, 6-dimethyl-1-benzofuran-3-yl) acetic acid (2DBAA): experimental and theoretical approach, J. Mol. Struct. 1171 (2018) 362–374.
[33] N. Kumar, K.M.M Udayabhanu, G. Nagaraju, Development and detection of level II and III features of latent fingerprints using highly sensitive AIE based coumarin fluorescent derivative, J. Sci. Adv. Mater. Devices 5 (2020) 520–526.
[34] M. Mohan, S. Pangannaya, M.N. Satyanarayan, D.R. Trived, Photophysical and electrochemical properties of organic molecules, solvatochromic effect and DFT studies, Opt. Mater. 77 (2018) 211–220.
[35] T. Sutradhar, A. Misra, Role of electron-donating and electron-withdrawing groups in tuning the optoelectronic properties of difluoroboron–napthyridine analogues, J. Phys. Chem. A 122 (16) (2018) 4111–4120.
[36] K. Upendranath, T. Venkatesh, Y. Arthoba Nayaka, M. Shashank, G. Nagaraju, Optoelectronic, DFT and current-voltage performance of new Schiff base 6-nitro-benzimidazole derivatives, Inorg. Chem. Commun. 139 (2022) 109354–109368.
[37] K.H. Ibnaouf, A.O. Elzupir, M.S. AlSalhi, A.S. Alaamer, Influence of functional groups on the photophysical properties of dimethylaminochalcones as laser dyes, J. Opt. Mater. 76 (2018) 216–221.
[38] A.A. Gabr, Spectrophotometric studies on some Schiff bases derived from benzidine, Spectrochim. Acta Part Mol. Spectrosc. 46 (1990) 1751–1757.
[39] E. Ermis, K. Durmus, Novel thiophene-benzothiazole derivative azomethine and amine compounds: microwave assisted synthesis, spectroscopic characterization, solvent effects on UV-Vis absorption and DFT studies, J. Mol. Struct. 1217 (2020) 128354–128360.
[40] M.M. Duvenhagel, O.M. Ntwaeborwal, H.G. Visser, H.C. Swart, The effect of electron donating and withdrawing groups on morphology and optical properties of Alq_3, J. Condens. Matter Phys. 439 (2014) 46–49.
[41] L. Leonat, S. Gabriela, I.V. Branzoi cyclic voltammetry for energy levels estimation of organic materilas, UPB Sci. Bull. Ser. B 75 (2013) 111–119.
[42] K.V. Basavarajappa, Y.A. Nayaka, R.O. Yathisha, Manjunatha, Synthesis, characterization, optical, electrochemical and current-voltage characteristics of coumarin dyes, J. Fluoresc. 29 (2019) 1201–1211.
[43] A. Becke, Density-functional exchange-energy approximation with correct asymptotic behavior, Phys. Rev. A 38 (1988) 3098–3100.
[44] A. Bendjeddou, T. Abbaz, A.K. Gouasmia, D. Villemin, Molecular structure, HOMO-LUMO, MEP and Fukui function analysis of some TTF-donor substituted molecules using DFT (B3LYP) calculations, Int. Res. J. Pure Appl. Chem. 12 (2016) 1–9.
[45] S. Muthu, J.C. Prasana, C.S. Abraham, M. Raja, Spectroscopic (FT-IR, FT-Raman) investigation, topology (ESP, ELF, LOL) analyses, charge transfer excitation and molecular docking (dengue, HCV) studies on ribavirin, Chem. Data Collect. 17 (2018) 236–250.
[46] H. Tanak, M. Toy, Molecular structure, spectroscopic and quantum chemical studies on 2′-chloro-4-dimethlamino azobenzene, J. Mol. Struct. 1068 (2014) 189–197.
[47] A. Mahmood, S.U. Khan, U.A Rana, M.R.S.A. Janjua, M.H. Tahir, M.F. Nazar, Y. Song, Effect of thiophene rings on UV/visible spectra and non-linear optical (NLO) properties of triphenylamine based dyes: a quantum chemical perspective, J. Phys. Org. Chem. 28 (2015) 418–422.
[48] M.I. Abdullah, M.R.S.A. Janjua, M.F. Nazar, A. Mahmood, Quantum chemical designing of efficient TC4-based sensitizers by modification of auxiliary donor and π-spacer, Bull. Chem. Soc. Jpn. 86 (2013) 1272-1281.
[49] A. Erdemir, S. Li, Y. Jin, Relation of certain quantum chemical parameters to lubrication behavior of solid oxides, Int. J. Mol. Sci. 6 (2005) 203–218.
[50] M.F. Nazar, A. Badshah, A. Mahmood, M.N. Zafar, M.R.S.A. Janjua, M.A. Razaa, R. Hussaind, Synthesis, spectroscopic characterization, and computed optical analysis of green fluorescent cyclohexenone derivatives, J. Phys. Org. Chem. 29 (2016) 152–160.
[51] S.M. Hiremath, A. Suvitha, N.R. Patil, C.S. Hiremath, S.S. Khemalapure, S.K. Pattanayak, K. Obelannavar, Molecular structure, vibrational spectra, NMR, UV, NBO, NLO, HOMO-LUMO and molecular docking of 2-(4, 6-dimethyl-1-benzofuran-3-yl) acetic acid (2DBAA): experimental and theoretical approach, J. Mole. Struct. 1171 (2018) 362–374.
[52] Y. Zhao, Z. Li, J. Liu, C. Hu, H. Zhang, B. Qin, Y. Wu, Intermolecular vibrational modes and H-bond interactions in crystalline urea investigated by terahertz spectroscopy and theoretical calculation, Spectrochim. Acta A Mol. Biomol. Spectrosc. 189 (2018) 528–534.
[53] M.D. Prabhu, J.T. Yenagi, V. Kamat, J. Tonannavar, XRD structure and vibrational analysis of DL-β-Leucine, as aided by DFT tetramer model and characterized by NBO, AIM and NCI calculations, J. Mol. Struct. 1218 (2020) 128495–128505.
[54] M.H.M. Krishnegowda, C.S. Karthik, P.J. Kudigana, P. Mallu, L.K. Neratur, μ-phenoxide bridged mixed ligand Cu (II) complex: synthesis, 3D supramolecular architecture, DFT, energy frameworks and antimicrobial studies, Polyhedron 185 (2020) 114571–114587.
[55] P. Hazarika, D.A. Russell, Advances in fingerprint analysis, Angew. Chem. Int. Ed. 51 (2012) 3524–3531.
[56] C. Huynh, J. Halamek, Forensic identification of gender from fingerprints, TrAC, Trends Anal. Chem. 82 (2016) 328–336.
[57] M.K. Priya, B.K. Revathi, V. Renuka, S. Sathya, P.S. Asirvatham, Molecular structure, spectroscopic (FT-IR, FT-Raman, ^{13}C and ^{1}H NMR) analysis, HOMO-LUMO energies, Mulliken, MEP and thermal properties of new chalcone derivative by DFT calculation, Mater. Today Proc. 8 (2019) 37–46.
[58] J. Lee, M.M. Joullié, Novel design and approach to latent fingerprint detection on paper using a 1,2-indanedione-based bi-functional reagent, Tetrahedron Lett. 56 (2015) 3378–3381.
[59] D. Navami, R.B. Basavaraj, S.C. Sharma, B.D. Prasad, H. Nagabhushana, Rapid identification of latent fingerprints, security ink and WLED applications of $CaZrO_3:Eu^{3+}$ fluorescent labelling agent fabricated via bio-template assisted combustion route, J. Alloy. Compd. 762 (2018) 763–779.
[60] D. Navami, R.B. Basavaraj, G.P. Darshan, H.K. Inamdar, S.C. Sharmac, H.B. Premkumar, H. Nagabhushana, Evolution of shapes and identification of level II and III features of fingerprints using $CaZrO_3:Sm^{3+}$ fluorescent markers prepared via solution combustion rout, J. Optic. Mater. 88 (2018) 479–487.
[61] M.C.P Ereshanaik, H.S. Bhojya Naik, B.R. Kirthan, H.M. Kumaraswamy, R. Sandeep Kumar Jain, DNA interaction studies of Cu (II), Co (II), and Ni (II) chelates derived from Schiff base ligand, J. Ind.Chem.Soc. 99 (2022) 100288–100290.